Journal of Alloys and Compounds 749 (2018) 803–810

Contents lists available at ScienceDirect

Journal of Alloys and Compounds

journal homepage: http://www.elsevier.com/locate/jalcom

Carbonized polydopamine wrapping layered KNb_3O_8 nanoflakes based on alkaline hydrothermal for enhanced and discrepant lithium storage

Qinglin Deng, Mengjiao Li, Junyong Wang, Kai Jiang**, Zhigao Hu*, Junhao Chu

Key Laboratory of Polar Materials and Devices (MOE) and Technical Center for Multifunctional Magneto-Optical Spectroscopy (Shanghai), Department of Electronic Engineering, East China Normal University, Shanghai 200241, China

ARTICLE INFO

Article history:
Received 1 December 2017
Received in revised form
1 March 2018
Accepted 27 March 2018
Available online 29 March 2018

Keywords:
KNb_3O_8
2D layered
Alkaline hydrothermal
Polydopamine
Lithium storage

ABSTRACT

Although the photochemical and ion exchange properties of layered KNb_3O_8 (KN) have been extensively studied, its potential lithium storage applications were ignored. Unlike typical acid hydrothermal method, this work demonstrate that interlayer-controlled KN nanoflakes can be prepared based on alkaline hydrothermal conditions. Pristine KN performs a high first-discharge capacity and superior cyclic stability. Moreover, polydopamine derived carbon as a conductive coating shell was firstly applied to modify KN for enhancing its lithium insertion ability. It performs outstanding rate character (310, 255, 110 mA h g^{-1} at the current density of 0.2, 1, 10 A g^{-1}, respectively), as compared with pristine KN (96, 51, 13 mA h g^{-1}). It also shows excellent long-term cycling feature (209 mA h g^{-1} after 3000 cycles, corresponds to 95% capacity retention). In addition, relevant energy storage mechanisms have been expounded. The present work could be helpful in developing potential multifunctional applications of KN-based and other similar niobates.

© 2018 Elsevier B.V. All rights reserved.

1. Introduction

As the pressing demand for preferable lithium ion batteries (LIBs), which has widespread applications in laptops, mobile phones and microelectronic devices, exploring novel anode materials for LIBs with excellent cycling and rate performances has surged [1–4]. Among them, two-dimensional (2D) materials such as metal chalcogenides, graphene and black phosphorus, have occupied the hotspots [5–7]. For example, the electrochemical properties of layered MoS_2 and SnS_2 have been extensively studied [8–10]. However, they possess a common shortcoming as the unstability under oxygen atmosphere and high temperature conditions. Remarkably, transition metal oxides, such as Nb_2O_5 and TiO_2, make amends for the disadvantage and show charming energy storage performances [1,11,12]. As a branch of them, 2D layered KNb_3O_8 (KN) should be worthy of attention. It possesses unique interlayer regions and has an orthorhombic crystal structure. The linked NbO_6 octahedral units form the 2D layered structure. Potassium ions between the layers keep the charge balance [13–16]. The unique interlayer features make it of great interest for applications in environmental purification, non-linear optics, energy conversion, etc. [17–21].

As a typical catalyst, there are some reports on the good photocatalytic activities of KN. However, most of them are focused on using acidic hydrothermal or traditional solid sintering technology to prepare KN [16,22–24]. The former would bring the potential ion exchange reaction between K^+ and H^+. The latter is hard to control the surface morphology. In view of the obvious advantage of hydrothermal method, it is significant to propose an alkaline hydrothermal approach. Although the photochemical and ion exchange properties of KN have been extensively studied [15,19,25,26], exploring the potential multifunctional KN-based applications would be an interesting topic. Considering the similar properties between niobium-based oxides and titanium-based anode materials, which have exhibited huge advantages in LIBs [27,28], it was believed that the layered KN could be as the potential anode active materials due to their unique layered structure and rich redox chemistry of Nb element [21]. The redox of Nb^{5+}/Nb^{4+} has the possibility to realize the reversible reaction with lithium, however,

* Corresponding author.
** Corresponding author.
E-mail addresses: kjiang@ee.ecnu.edu.cn (K. Jiang), zghu@ee.ecnu.edu.cn (Z. Hu).

https://doi.org/10.1016/j.jallcom.2018.03.337
0925-8388/© 2018 Elsevier B.V. All rights reserved.

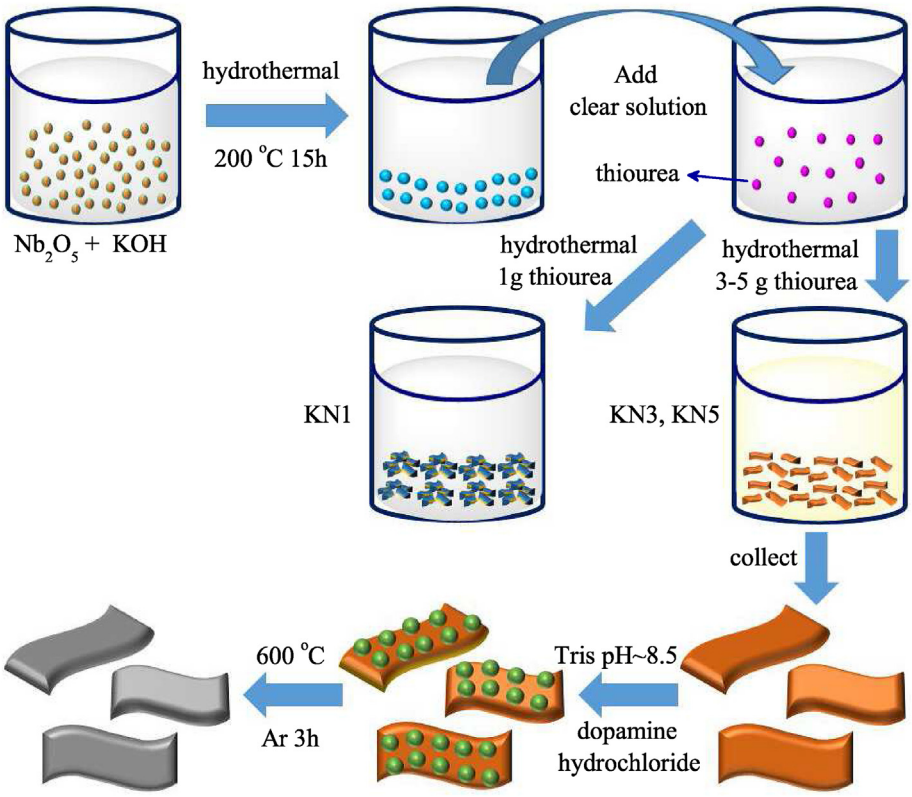

Fig. 1. Schematic illustration of the synthesis process for KN1, KN3, KN5, KN3@C and KN5@C.

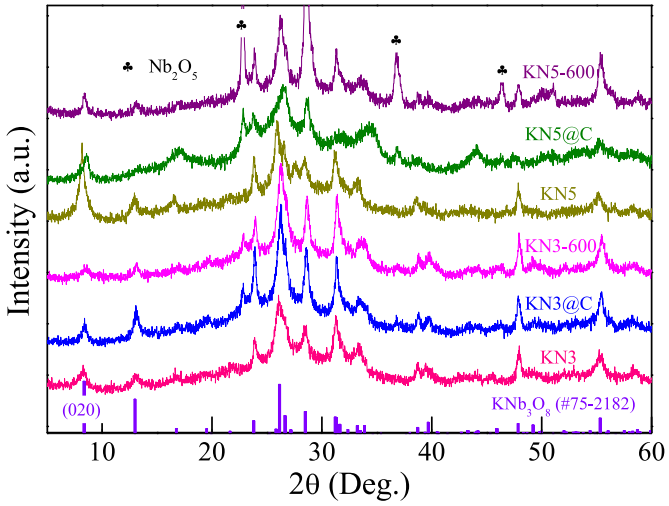

Fig. 2. (a) XRD patterns of KN3, KN3@C, KN3-600, KN5, KN5@C and KN5-600.

the poor electrical conductivity restricts the exertion of LIBs performances [1,11,29]. An efficient approach to address this issue is to composite KN with conductive materials, such as carbon as a conductive coating shell. It was reported that polydopamine can strongly attach to diverse surfaces with high binding strength. It has high conductivity after carbonization, with controllable film thickness [30–34]. To be our best knowledge, compositing KN with polydopamine for the applications in LIBs has not yet been reported.

In this work, we devoted to propose an alkaline hydrothermal strategy to prepare KN. Remarkably, interlayer-controlled KN nanoflakes can be obtained in the aid of adding different amount of thiourea. Pristine KN performs a high first discharge capacity but poor rate features. Moreover, polydopamine derived carbon has been used to improve the electrochemical performances of KN. As for the applications in LIBs, it shows superior cycling and rate performances. In addition, relevant kinetics mechanisms have been expounded. It is believed that the present work could be helpful in further understanding the intrinsic lithium insertion features of KN and developing its potential energy storage applications.

2. Experimental details

2.1. Preparation of KN3, KN5, KN3@C and KN5@C

In this work, pristine KN nanoflakes were prepared under alkaline hydrothermal conditions. Typically, the resulting mixture of 2.4 g Nb_2O_5 and 80 mL 0.9 mol L^{-1} KOH solution was transferred into a polytetrafluoroethylene-lined stainless autoclave and hydrothermally treated at 200 °C for 12 h. Then 1, 3, and 5 g of thiourea (for short as KN1, KN3, and KN5, respectively) were added into 30 mL of the above resulting clear solution. After hydrothermally treated at 200 °C for 15 h, the final products were collected, then washed with deionized (DI) water and absolute ethanol for several times, finally dried at 80 °C in vacuum for 20 h.

In order to improve the electrical conductivity, the as-prepared KN5 and KN3 nanoflakes was modified using polydopamine as a carbon source, abbreviated as KN5@C and KN3@C, respectively. Typically, 0.2 g of the previously prepared KN5 was added into 160 mL of Tris-buffer (10 mmol L^{-1}) by ultrasonic dispersion for 30 min. Then it was stirred to ensure homogeneous suspension. Subsequently, 160 mg of dopamine hydrochloride was added into the suspension under constant magnetic stirring at room

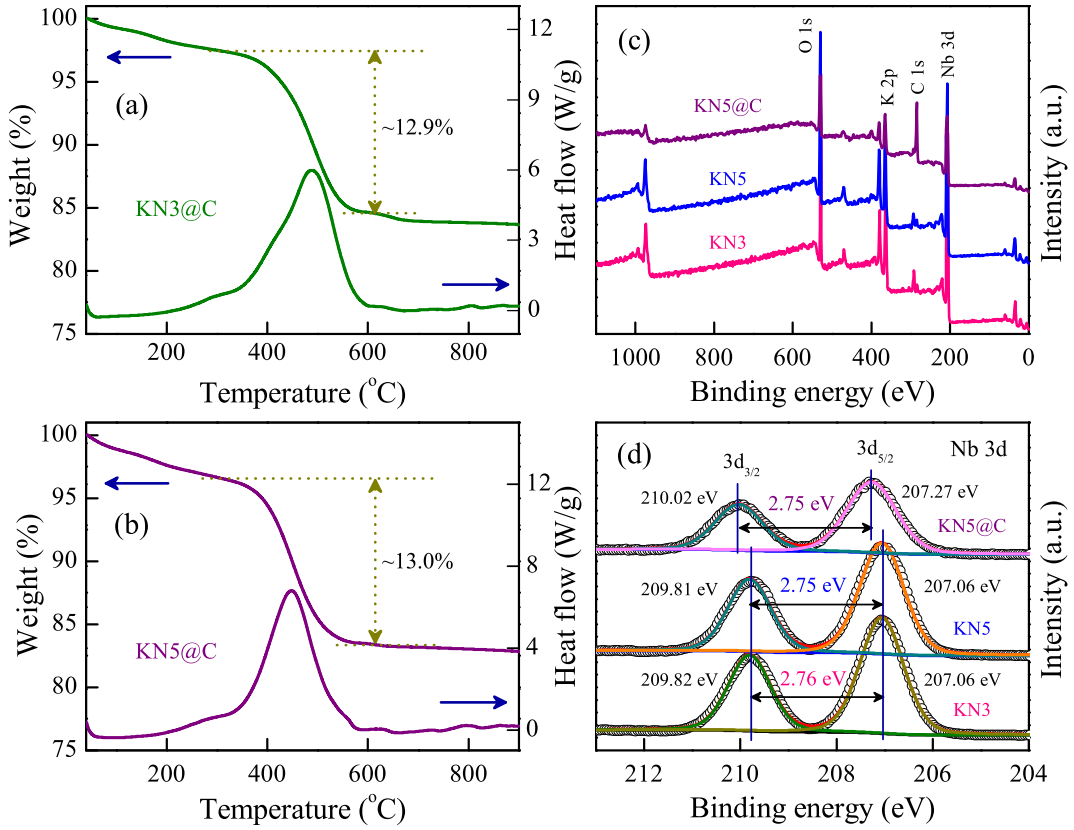

Fig. 3. TGA-DSC analyses of (a) KN3@C and (b) KN5@C. (c) The typical overall XPS spectrum of KN3, KN5 and KN5@C. (d) High-resolution XPS spectra of Nb 3d for KN3, KN5 and KN5@C.

temperature for 48 h. Note that the pH of mixture was controlled at about 8.5. After that, the resulting product was extracted by centrifugation and washed repeatedly with DI water, then dried in a vacuum oven at 80 °C for 24 h. To obtain KN5@C, the KN5@polydopamine sample was heated to 600 °C for 3 h under argon atmosphere. KN3@C was prepared by following the same procedures. In addition, as a comparison, pristine KN5 and KN3 were also heated to 600 °C for 3 h under argon atmosphere, abbreviated as KN5-600 and KN3-600, respectively.

2.2. Characterization methods

The crystal structures of all samples were investigated by X-ray diffraction (XRD, Cu Kα, D8 Advance, Bruker). Thermogravimetric analyses (TGA) and differential scanning calorimetry (DSC) of samples were analyzed in a TGA/DSC 1 STAR^e System (Mettler-Toledo) from 40 °C to 900 °C with a heating rate of 15 °C min^{-1}. X-ray photoelectron spectroscopy (XPS) measurements were carried out on a Thermo ESCALAB 250XI system with Al-Kα radiation ($h\nu$ = 1486.6 eV). The surface morphologies of powder samples were acquired by field emission scanning electron microscopy (FEI Quanta 400 FEG). The transmission electron microscopy (TEM) images and selected area electron diffraction (SAED) were performed by TEM (FEI Tecnai G2 F20) with an acceleration voltage of 200 kV, equipped with an energy dispersive X-ray spectroscopy (EDX) detector for elemental mapping.

2.3. Lithium ion batteries tests

Two-electrode coin-cell (CR-2025) assembled in an argon-filled glovebox were used for the energy storage investigation. The as-prepared samples were used as the working electrode, which was fabricated by casting a slurry of 80 wt% active material, 10 wt% acetylene black, and 10 wt% polyvinylidene fluoride in *N*-methyl-2-pyrrolidinone (NMP) on a copper foil, then dried at 100 °C in vacuum for 24 h. The lithium foil was used as counter and reference electrodes, a membrane (Celgard 2400) as the separator, and the electrolytes were 1 mol L^{-1} $LiPF_6$ solution in a 1:1:1 (by volume) mixture of ethylene carbonate (EC), dimethyl carbonate (DMC) and ethyl methyl carbonate (EMC). Galvanostatic charge-discharge experiments were performed at different current densities in the voltage range of 0.02–3.0 V (*vs.* Li^+/Li) using battery measurement system (LAND-CT2001A). Cyclic voltammetry (CV), and electrochemical impedance spectroscopy (EIS) were performed on an electrochemical workstation (CHI660E). All electrochemical measurements were carried out at room temperature.

3. Results and discussion

3.1. Schematic illustration of preparation

The typical synthetic procedures for KN1, KN3, KN5, KN3@C and KN5@C were schematically illustrated in Fig. 1. The initial hydrothermal reaction of Nb_2O_5 and KOH can prepare the layered $K_4Nb_6O_{17}$. However, the raw materials were incompletely used. Our previous study has demonstrated that $K_4Nb_6O_{17}$ can be synthesized by adding urea into the resulting clear solution [28]. In the work, it was found that the different amount of thiourea plays a key role in the preparation of KN. A small quantity of $K_4Nb_6O_{17}$ was obtained when adding inadequate thiourea into the clear solution. As increasing the amount of thiourea, KN nanoflakes can be successfully prepared. It is noteworthy that the pH of all hydrothermal

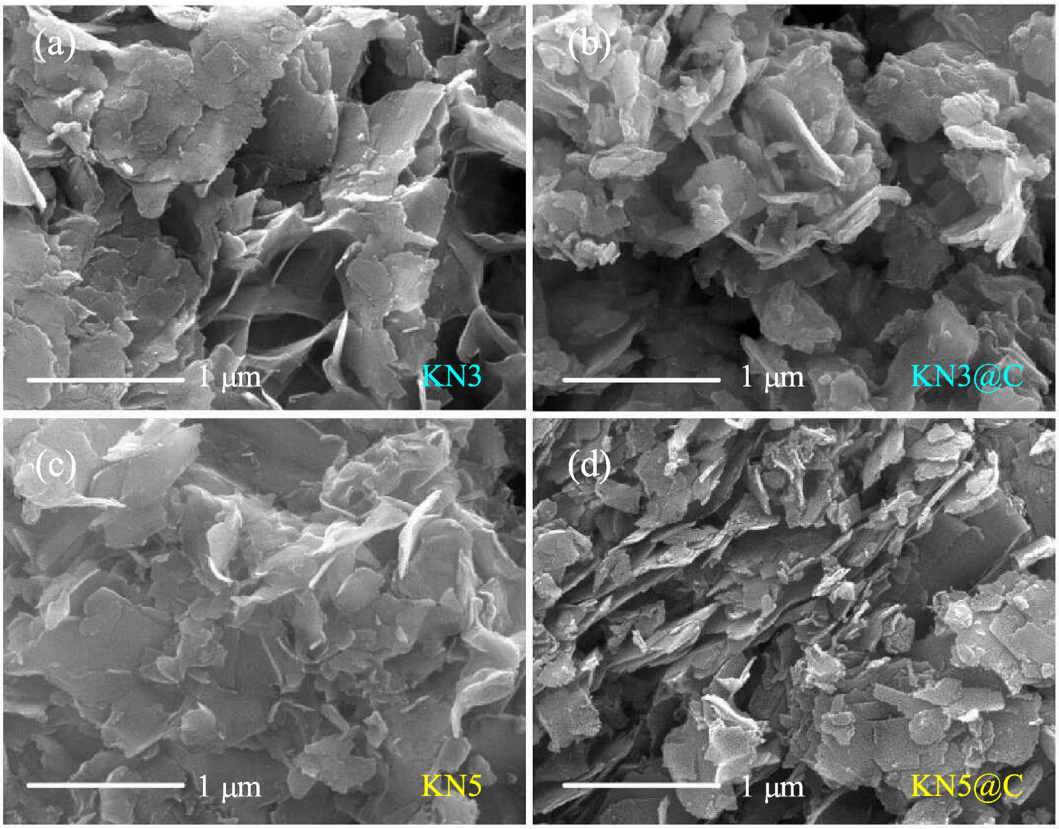

Fig. 4. SEM images of (a) KN3, (b) KN3@C, (c) KN5 and (d) KN5@C under different magnifications.

resulting solutions are alkaline. In order to improve the electrical conductivity, dopamine as a carbon source can strongly attach to the surface of KN nanoflakes in the Tris-buffer solution. After magnetic stirring, being dried and thermal treatment, the KN5@C and KN3@C was obtained.

3.2. XRD, TGA and XPS analysis

Fig. 2 shows the X-ray diffraction (XRD) patterns of as-prepared samples. It was found that the diffraction peaks of KN3 and KN5 can be assigned to the orthorhombic phase of KNb_3O_8 with lattice constants $a = 8.903$ Å, $b = 21.16$ Å, and $c = 3.799$ Å (JPCDS No. 75-2182). Note that the (020) diffraction peaks are characteristic of the layered structures of KN. As we can see, the intensity of the (020) peak for KN5 is higher than that of KN3, indicating that KN5 was preferred orientation along the (020) peak to grow. The diffraction peaks of the KN5@C and KN3@C composites were similar to those of pure KN5 and KN3 except for the peaks of Nb_2O_5. In addition, the peak intensity corresponds to (020) decreases for KN5@C compared to KN5. Because the (020) peak is easily effected by external factors, such as temperature and humidity. As a result, during the process of annealing, the preferred (020) peak of KN5 was more easily destroyed. However, for KN3 and KN3@C, the intensity of the (020) peak for KN3 is weak. The peak intensity corresponds to (020) slightly increases for KN3@C compared to KN3. The reason might be attributed to the temperature effects, which leads to the enhanced crystallinity. Note that a small quantity of Nb_2O_5 impurity was inevitably generated due to the volatilization of alkali metal ions during the process of annealing. However, this impurity plays a key role in enhancing the electrical performance of KN5@C (seen in the subsection of Energy Storage Applications). Due to lack of the protection of carbon layers, there is more Nb_2O_5 generated in KN5-600 and KN3-600.

The stability and carbon content of KN3@C and KN5@C were confirmed by TGA-DSC, as shown in Fig. 3a and b. As we can see, both of them exhibit one distinctive weight loss stage with an endothermic peak, which takes place in the temperature range of 250–600 °C. The weight percentage of carbon in KN3@C and KN5@C based on TGA-DSC analysis was estimated to be about 12.9 wt% and 13.0 wt%, respectively. Fig. 3c shows the typical overall XPS spectrum of KN3, KN5 and KN5@C. C, Nb and O elements can be detected on the surface. High-resolution XPS spectra of Nb 3d were shown in Fig. 3d. It was found that the XPS spectra of KN3 and KN5 were basically the same. As an example, the Nb 3d XPS spectra of KN5 were observed at 209.81 eV and 207.06 eV for the $3d_{3/2}$ and $3d_{5/2}$ peaks, respectively, and the distance between the two peaks is 2.75 eV. This suggests that the Nb ion is in the 5+valence state [35]. After combining with carbon, the binding energy of $3d_{3/2}$ and $3d_{5/2}$ peaks shift toward a higher energy. However, the distance between these two peaks of Nb 3d for KN5@C remains the same value of 2.75 eV.

3.3. Surface morphologies

The morphologies of the as-synthesized samples were characterized by scanning electron microscopy (SEM). As shown in Fig. 4a and c, both of KN3 and KN5 have the similar morphologies. It was found that they are composed of thin nanoflakes, which pack densely and show a porous structure. As depicted by Fig. 4b and d, for KN3@C and KN5@C, after combining with carbon, the surface of KN3 and KN5 became rough. Moreover, the microstructural information of KN3@C and KN5@C was further characterized by

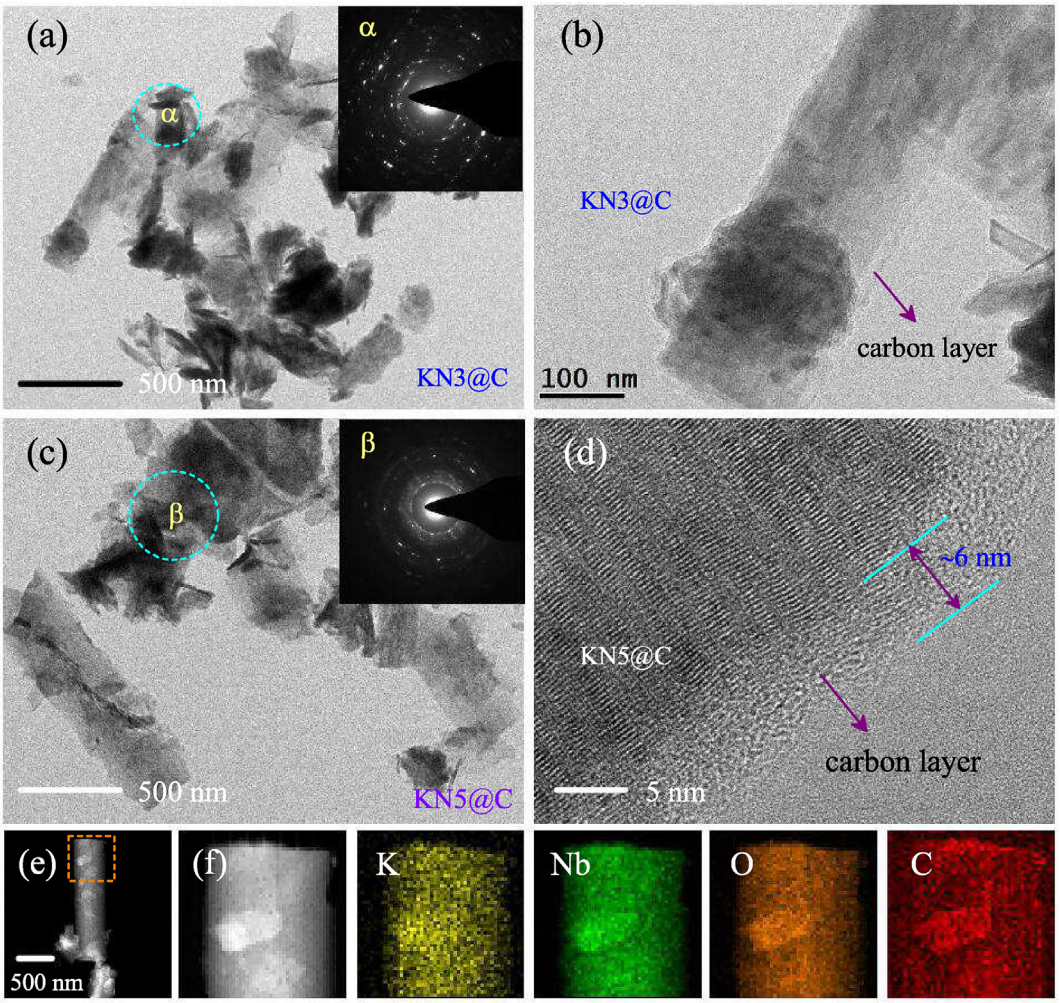

Fig. 5. TEM images of (a)–(b) KN3@C and (c)–(d) KN5@C under different magnifications, with the corresponding SAED patterns. (e)–(f) TEM images of KN5@C with elemental mapping of K, Nb, O, and C.

transmission electron microscopy (TEM), and the corresponding selected area electron diffraction (SAED) image is also provided. Fig. 5a–d shows the TEM images of KN3@C and KN5@C. It remains the similar nanoflakes morphologies after combining with carbon. It can be found that the polydopamine derived carbon layers are tightly wrapped onto the surface of KN3 and KN5 nanoflakes. As an example, the carbon layers of KN5@C are about 6 nm, as shown in Fig. 5d. The SEAD patterns (shown in Fig. 5a and c) further prove the mixed-phase nature of single crystal KN (bright diffraction spots) and the massive accumulation of carbon (diffraction rings). Moreover, in order to investigate the detailed local elemental composition and distribution of KN5@C, the corresponding energy dispersive X-ray (EDX) mapping experiments have been carried out. Fig. 5e and f shows the corresponding TEM images of KN5@C. From the EDX mapping analysis, it further verifies the uniform distribution of K, Nb, O and C elements.

3.4. Energy storage applications

Owing to the unique layer structure and NbO_6 octahedron of KN, it possesses the potential ability to realize the reversible reaction with lithium. In the work, two-electrode coin-cell has been adopted to investigate the potential energy storage applications of KN-based samples, which were as anode materials for the LIBs. Note that the root-mean-square (RMS) surface roughness of copper foil is about 380 nm investigated by atomic force microscopy (not shown). Copper foil with small surface roughness is ideally good for the LIBs, bringing excellent electrochemical performances. Fig. 6a–c shows the typical cyclic voltammetry (CV) curves of KN3, KN5 and KN5@C, respectively, for the initial ten cycles in the voltage range of 0.02–3.0 V at a sweep rate of 0.5 mV s^{-1}. For KN5, the reduction peak is observed at around 1.27 V *vs.* Li^+/Li during the first reduction process (Li insertion), and the oxidation peaks are broad and unobvious during the first oxidation process (Li extraction). The subsequent curves except for the second cycle show quite good reproducibility. KN3 has the similar CV results. For KN5@C, it exhibits broad cathodic and anodic peaks. The reduction peaks are observed at around 0.52, 1.25 and 1.49 V *vs.* Li^+/Li during the first reduction process, and the oxidation peaks are observed at about 1.19, 1.48 and 2.28 V *vs.* Li^+/Li during the first oxidation process. The subsequent reduction peaks shift to higher potential *vs.* Li^+/Li with increasing the cycle number. It is significant to explore the kinetic mechanisms of Li-ion insertion/extraction behaviors for KN5@C. Fig. 6d shows the CV results with various sweep rates. As we know, the CV curves follows the power law: $i = av^b$, where a and b are adjustable parameters, i is the current, and v is the sweep rate. The value of b is close to 0.5 and 1, corresponds to the diffusion-limited contribution and surface-controlled pseudocapacitive reaction,

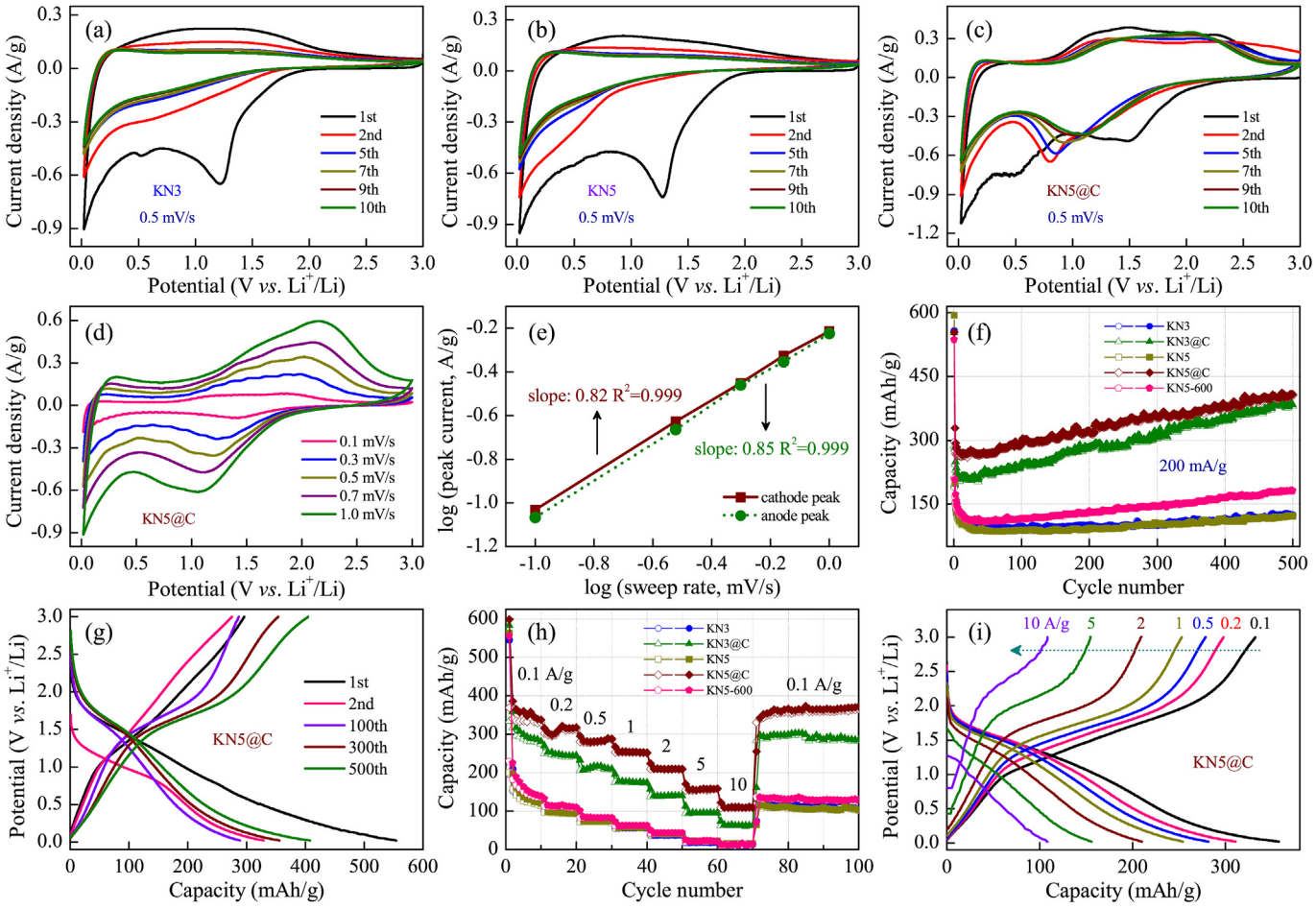

Fig. 6. Cyclic voltammetry (CV) curves of (a) KN3, (b) KN5 and (c) KN5@C measured at a scan rate of 0.5 mV s^{-1} in the voltage range of 0.02–3.0 V (*vs.* Li^+/Li). (d) CV curves of KN5@C measured at various sweep rates from 0.1 to 1.0 mV s^{-1} with (e) the corresponding specific peak current, in the voltage range of 0.02–3.0 V (*vs.* Li^+/Li). (f) Cycling stability of KN3, KN3@C, KN5, KN5@C and KN5-600 at a current density of 200 mA g^{-1}. (g) Galvanostatic charge-discharge (GCD) profiles of KN5@C at 200 mA g^{-1} for 500 cycles. (h) Rate performance of KN3, KN3@C, KN5, KN5@C and KN5-600 at different current densities. (i) GCD profiles of KN5@C at different rates.

respectively. Fig. 6e shows the specific peak current of KN5@C at different sweep rates. As we can see, the *b* values based on anode and cathode peak currents for KN5@C are close to 1, which demonstrates that the kinetic of lithium storage for KN5@C is mainly derived from surface-controlled pseudocapacitive reaction.

The cycling performances of all KN-based samples were evaluated at a constant current density of 200 mA g^{-1}, as presented in Fig. 6f. As we can see, the first discharge capacity of all samples reach a high value of around 550 mA h g^{-1}, then they dramatically fade during a few dozen cycles, which is in good agreement with the CV results. For KN3 and KN5, they show the similar cycling performances. For instance, the discharge capacity have a slight increase after 500 cycles, as compared with the value at 20th cycle. For KN5-600, a small quantity of Nb_2O_5 impurity in it can influence its cycling performances. The discharge capacity at the 500th is about 181 mA h g^{-1}, which is much higher than the value at 20th cycle (about 115 mA h g^{-1}). For KN3@C and KN5@C, they did the best cycling performances. In detail, the discharge capacity of KN3@C and KN5@C at the 20th is about 213 and 269 mA h g^{-1}, respectively. As discussed in XRD analysis, after annealing, KN5@C generated more Nb_2O_5 impurity than KN3@C, which might results in the higher capacity for KN5@C. After 500 cycles, the values increase to 383 and 408 mA h g^{-1}. The phenomenon was similar to KN5-600. The reason might be attributed to the complex activation process derived from KN and Nb_2O_5 impurity. Moreover, as a typical example, Fig. 6g displays the galvanostatic charge-discharge (GCD) curves in the 1st, 2nd, 100th, 300th and 500th cycles for the KN5@C electrode. As we can see, KN5@C reveals considerable discharge specific capacities of about 554 mA h g^{-1} in the first cycle but with a low coulombic efficiency. The inapparent discharge plateaus can be observed at around 1.5 V *vs.* Li^+/Li, which is in accordance with the above CV study. While the nature of the initial irreversible capacity is still unclear, the electrolyte decomposition, destructive structure or irreversible reaction might lead to the phenomenon.

Rate performance is one of the most important features to evaluate the LIBs. Fig. 6h shows the evolution of the specific capacity for all samples at different current densities. KN3, KN5 and KN5-600 have the similar rate character, with a low specific capacity at various rates. Remarkably, after combining with carbon, the specific capacity of KN3@C and KN5@C dramatically increase. KN5@C possesses a better rate performance, as compared with KN3@C. Concretely, it has a highest specific capacity of about 360 mA h g^{-1} than others at the current density of 0.1 A g^{-1}. With increasing the current density, the specific capacities of KN5@C gradually decrease. When the current density increases to 10 A g^{-1}, it still has a specific capacity of about 110 mA h g^{-1}. Then a specific capacity of 362 mA h g^{-1} can be maintained when the current density comes back again to 0.1 A g^{-1}, which suggests an excellent reversibility and cyclic stability of KN5@C electrode. Correspondingly, Fig. 6i presents the typical GCD profiles of KN5@C electrode at

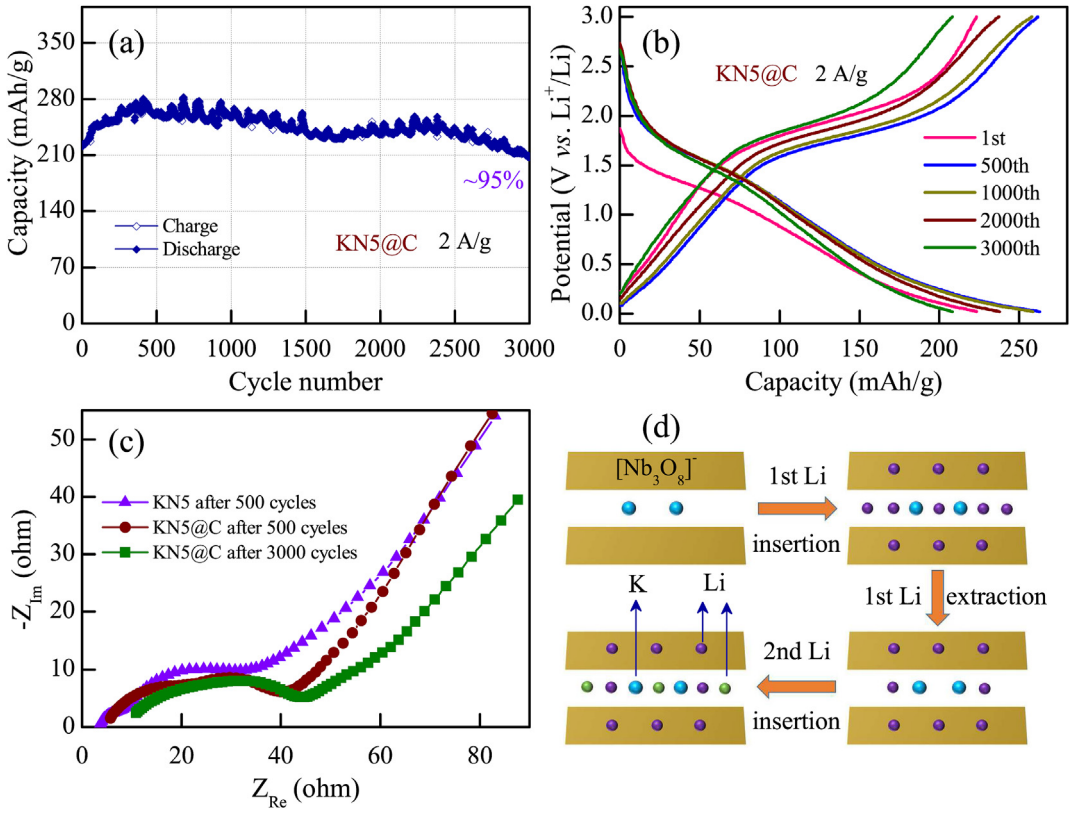

Fig. 7. (a) Cycling stability of KN5@C at 2 A g^{-1} rate with (b) the corresponding GCD profiles. (c) Nyquist plots of KN5 and KN5@C after 500th cycle (at a current density of 0.2 A g^{-1}), and KN5@C after 3000th cycle (at a current density of 2 A g^{-1}), in the frequency range of 100 kHz to 0.1 Hz. (d) The possible mechanisms of lithium ion insertion/extraction for KN.

different current densities in range of 0.1–10 A g^{-1}. The specific capacity of KN5@C decreases with increasing charge-discharge current densities. Considering the low specific capacity and rate performance of KN5-600, it was believed that the excellent energy storage performances of KN5@C were derived from the combined actions of carbon and Nb_2O_5 impurity.

Moreover, the cyclic stability of the activated KN5@C electrode at a high current density of 2 A g^{-1} has been investigated. As shown in Fig. 7a, KN5@C still possesses a high specific capacity of about 209 mA h g^{-1} after 3000 cycles, which corresponds to 95% capacity retention, as compared with the value at the first cycle. Correspondingly, Fig. 7b presents the typical GCD profiles at the 1th, 500th, 1000th, 2000th and 3000th cycle. These curves are similar to each other. The admirable long-term cycling performance of KN5@C demonstrates the potential energy storage applications. In addition, the electrochemical impedance spectra (EIS) of KN5 and KN5@C after 500th cycle (at a current density of 0.2 A g^{-1}), and KN5@C after 3000th cycle (at a current density of 2 A g^{-1}) are compared in Fig. 7c. It was found that KN5@C after 3000th cycle has a larger contact resistance at high frequency than others. All of them have a low charge transfer resistance at medium frequency with a similar semicircle. The straight line at low frequency represents the mass transfer of lithium ions. KN shows the interesting and complicated Li insertion/extraction reactions. In the work, the possible mechanisms of lithium ions insert/extract into KN have been depicted in Fig. 7d. As we know, KN is composed of octahedral units of NbO_6 and possesses a typical 2D layered structure. The specific capacity might be mainly derived from the two reaction mechanisms. One is the valence variation of Nb^{5+} to Nb^{4+}, the other is the complicated solid-solution reaction of Li and KN. We speculate that the reason for the low reversible capacity might be due to the lack of Li^+ insertion sites in the KN crystal structure and low electrical conductivity.

4. Conclusion

In conclusion, interlayer-controlled KN nanoflakes have been successfully prepared using alkaline hydrothermal method with the aid of thiourea. Pristine KN performs a superior cyclic stability but poor rate features. Polydopamine derived carbon and Nb_2O_5 impurity have been proved to deeply influence the energy storage performances of KN. As for the application in LIBs, it performs excellent rate feature. For instance, it still possesses a high specific capacity of about 110 mA h g^{-1} at the current density of 10 A g^{-1}, as compared with the 0.2 A g^{-1} rate (about 310 mA h g^{-1}). It also exhibits outstanding cyclic stability with a capacity retention of ~95% after 3000 cycles. This work shows novel insights into KN, including the alkaline hydrothermal preparation strategy, polydopamine modification and lithium insertion behavior, which could be helpful in broadening the multifunctional applications of KN and other similar layered niobates.

Acknowledgments

This work was financially supported by National Key Research and Development Program of China (Grant No. 2017YFA0303403), Natural Science Foundation of China (Grant Nos. 61674057, 61504156, and 61227902), Projects of Science and Technology Commission of Shanghai Municipality (Grant No. 15JC1401600), and the Program for Professor of Special Appointment (Eastern Scholar) at Shanghai Institutions of Higher Learning and the Fundamental Research Funds for the Central Universities.

References

[1] H.T. Sun, L. Mei, J.F. Liang, Z.P. Zhao, C. Lee, H.L. Fei, M.N. Ding, J. Lau, M.F. Li, C. Wang, X. Xu, G.L. Hao, B. Papandrea, I. Shakir, B. Dunn, Y. Huang, X.F. Duan, Three-dimensional holey-graphene/niobia composite architectures for ultrahigh-rate energy storage, Science 356 (2017) 599–604.

[2] N. Mahmood, T. Tang, Y. Hou, Nanostructured anode materials for lithium ion batteries: progress, challenge and perspective, Adv. Energy Mater. 6 (2016), 1600374.

[3] N. Nitta, D. Lei, H.R. Jung, D. Gordon, E. Zhao, G. Gresham, J. Cai, I. Luzinov, G. Yushin, Influence of binders, carbons, and solvents on the stability of phosphorus anodes for Li-ion batteries, ACS Appl. Mater. Interfaces 8 (2016) 25991–26001.

[4] H. Yu, H. Lan, L. Yan, S. Qian, X. Cheng, H. Zhu, N. Long, M. Shui, J. Shu, $TiNb_2O_7$ hollow nanofiber anode with superior electrochemical performance in rechargeable lithium ion batteries, Nanomater. Energy 38 (2017) 109–117.

[5] W. Xu, T. Wang, S. Wu, S. Wang, N-doped carbon-coated MoS_2 nanosheets on hollow carbon microspheres for high-performance lithium-ion batteries, J. Alloys Compd. 698 (2017) 68–76.

[6] M.S. Xu, T. Liang, M.M. Shi, H.Z. Chen, Graphene-like two-dimensional materials, Chem. Rev. 113 (2013) 3766–3798.

[7] G.L. Xu, Z.H. Chen, G.M. Zhong, Y.Z. Liu, Y. Yang, T.Y. Ma, Y. Ren, X.B. Zuo, X.H. Wu, X.Y. Zhang, K. Amine, Nanostructured black phosphorus/ketjenblack-multiwalled carbon nanotubes composite as high performance anode material for sodium-ion batteries, Nano Lett. 16 (2016) 3955–3965.

[8] B. Zhao, Z. Wang, Y. Gao, L. Chen, M. Lu, Z. Jiao, Y. Jiang, Y. Ding, L. Cheng, Hydrothermal synthesis of layer-controlled MoS_2/graphene composite aerogels for lithium-ion battery anode materials, Appl. Surf. Sci. 390 (2016) 209–215.

[9] Q. Pang, Y. Zhao, X. Bian, Y. Ju, X. Wang, Y. Wei, B. Liu, F. Du, C. Wang, G. Chen, Hybrid graphene@MoS_2@TiO_2 microspheres for use as a high performance negative electrode material for lithium ion batteries, J. Mater. Chem. A 5 (2017) 3667–3674.

[10] L. Yin, S. Chai, J. Ma, J. Huang, X. Kong, P. Bai, Y. Liu, Effects of binders on electrochemical properties of the SnS_2 nanostructured anode of the lithium-ion batteries, J. Alloys Compd. 698 (2017) 828–834.

[11] K.J. Griffith, A.C. Forse, J.M. Griffin, C.P. Grey, High-rate intercalation without nanostructuring in metastable Nb_2O_5 bronze phases, J. Am. Chem. Soc. 138 (2016) 8888–8899.

[12] J. Li, J. Huang, J. Li, L. Cao, H. Qi, Y. Cheng, Q. Xi, H. Dang, Improved Li-ion diffusion process in TiO_2/rGO anode for lithium-ion battery, J. Alloys Compd. 727 (2017) 998–1005.

[13] P.M. Gasperin, Structure du triniobate(V) de potassium KNb_3O_8, un niobate lamellaire, Acta Crystallogr. B38 (1982) 2024–2026.

[14] A. Kudo, T. Sakata, Effect of ion exchange on photoluminescence of layered niobates $K_4Nb_6O_{17}$ and KNb_3O_8, J. Phys. Chem. C 100 (1996) 17323–17326.

[15] B. Liang, N. Zhang, C. Chen, X. Liu, R. Ma, S. Tong, Z. Mei, V.A.L. Roy, H. Wang, Y. Tang, Hierarchical yolk-shell layered potassium niobate for tuned pH-dependent photocatalytic H_2 evolution, Catal. Sci. Technol. 7 (2017) 1000–1005.

[16] X. Liu, W. Que, L.B. Kong, Hydrothermal synthesis of bamboo-shaped nanosheet KNb_3O_8 with enhanced photocatalytic activity, J. Alloys Compd. 627 (2015) 117–122.

[17] G. Zhang, J. Gong, X. Zou, F. He, H. zhang, Q. Zhang, Y. Liu, X. Yang, B. Hu, Photocatalytic degradation of azo dye acid red G by KNb_3O_8 and the role of potassium in the photocatalysis, Chem. Eng. J. 123 (2006) 59–64.

[18] L. Li, J. Deng, R. Yu, J. Chen, X. Wang, X. Xing, Phase evolution in low-dimensional niobium oxide synthesized by a topochemical method, Inorg. Chem. 49 (2010) 1397–1403.

[19] A. Waroquet, V. Demange, N. Hakmeh, J. Perrière, S. Freslon, S. Députier, M. Guilloux-Viry, Epitaxial growth and cationic exchange properties of layered KNb_3O_8 thin film, RSC Adv. 7 (2017) 15482–15491.

[20] B. Yu, B. Cao, H. Cao, X. Zhang, D. Chen, J. Qu, H. Niu, Synthesis and nonlinear optical properties of single-crystalline KNb_3O_8 nanowires, Nanotechnology 24 (2013), 085704.

[21] H. Nakayama, M. Nose, S. Nakanishi, H. Iba, Electrochemical reactions of layered niobate material as novel anode for sodium ion batteries, J. Power Sources 287 (2015) 158–163.

[22] J.F. Liu, X.L. Li, Y.D. Li, Synthesis and characterization of nanocrystalline niobates, J. Cryst. Growth 247 (2003) 419–424.

[23] G. Zhang, F. He, X. Zou, J. Gong, H. Tu, H. Zhang, Q. Zhang, Y. Liu, Hydrothermal synthesis and photocatalytic property of KNb_3O_8 with nanometer leaf-like network, J. Alloys Compd. 427 (2007) 82–86.

[24] X. Kong, D. Hu, P. Wen, T. Ishii, Y. Tanaka, Q. Feng, Transformation of potassium Lindquist hexaniobate to various potassium niobates: solvothermal synthesis and structural evolution mechanism, Dalton Trans. 42 (2013) 7699–7709.

[25] J. Sun, L. Liu, X.L. Zhao, S.L. Yang, S. Komarnenic, D.J. Yang, Capture of radioactive cations from water using niobate nanomaterials with layered and tunnel structures, RSC Adv. 5 (2015) 75354–75359.

[26] X. Zhang, M. Wang, D. Li, L. Liu, J. Ma, J. Gong, X. Yang, X. Xu, Z. Tong, Electrochemical investigation of a novel metalloporphyrin intercalated layered niobate modified electrode and its electrocatalysis on ascorbic acid, J. Solid State Electrochem. 17 (2013) 3177–3184.

[27] H. Ge, T.T. Hao, H. Osgood, B. Zhang, L. Chen, L.X. Cui, X.M. Song, O. Ogoke, G. Wu, Advanced mesoporous spinel $Li_4Ti_5O_{12}$/rGO composites with increased surface lithium storage capability for high-power lithium-ion batteries, ACS Appl. Mater. Interfaces 8 (2016) 9162–9169.

[28] Q.L. Deng, M.J. Li, J.Y. Wang, P. Zhang, K. Jiang, J.Z. Zhang, Z.G. Hu, J.H. Chu, Boosted adsorption-photocatalytic activities and potential lithium intercalation applications of layered potassium hexaniobate nano-family, RSC Adv. 7 (2017) 28105–28113.

[29] C. Pham, J.H. Choi, J. Yun, A.S. Bandarenka, J. Kim, P.V. Braun, S.Y. Jeong, C.R. Cho, Synergistically enhanced electrochemical performance of hierarchical MoS_2/$TiNb_2O_7$ hetero-nanostructures as anode materials for Li-ion batteries, ACS Nano 11 (2017) 1026–1033.

[30] G.P. Maier, M.V. Rapp, J.H. Waite, J.N. Israelachvili, A. Butler, Adaptive synergy between catechol and lysine promotes wet adhesion by surface salt displacement, Science 349 (2015) 628–632.

[31] Y. Liu, K. Ai, L. Lu, Polydopamine and its derivative materials: synthesis and promising applications in energy, environmental, and biomedical fields, Chem. Rev. 114 (2014) 5057–5115.

[32] Y. Ji, J.L. Li, S.F.Y. Li, Synergistic effect of the bifunctional polydopamine-Mn_3O_4 composite electrocatalyst for vanadium redox flow batteries, J. Mater. Chem. A 5 (2017) 15154–15166.

[33] B.B. Jiang, Y.J. He, B. Li, S.Q. Zhao, S. Wang, Y.B. He, Z.Q. Lin, Polymer-templated formation of polydopamine-coated SnO_2 nanocrystals: anodes for cyclable lithium-ion batteries, Angew. Chem. Int. Ed. 56 (2017) 1–5.

[34] B.P. Lee, P.B. Messersmith, J.N. Israelachvili, J.H. Waite, Mussel-inspired adhesives and coatings, Annu. Rev. Mater. Res. 41 (2011) 99–132.

[35] Q.L. Deng, M.J. Li, J.Y. Wang, P. Zhang, K. Jiang, J.Z. Zhang, Z.G. Hu, J.H. Chu, Exploring optoelectronic properties and mechanisms of layered ferroelectric $K_4Nb_6O_{17}$ nanocrystalline films and nanolaminas, Sci. Rep. 7 (2017) 1883.